Modeling and optimization of artificial magnetic conductor on the performance of on-chip-antenna for 28 GHz devices

Ahmadu Girgiri[1], Mohd Fadzil Ain[1], Mohd Zamir Pakhuruddin[2], Mohamad Faiz Mohamed Omar[3,4], Bello Muhammad Abdullahi[1]

[1]School of Electrical and Electronic Engineering, Universiti Sains Malaysia, Pulau Pinang, Malaysia
[2]School of Physic, Universiti Sains Malaysia, Pulau Pinang, Malaysia
[3]Collaborative Microelectronic Design Excellence Center (CEDEC), Sains@USM, Persiaran Bukit Jambul, Pulau Pinang, Malaysia
[4]Wireless Communication Centre (WCC), Faculty of Electrical Engineering, Universiti Teknologi Malaysia, Johor, Malaysia

Article Info

ABSTRACT

The growing popularity of chip-based devices has spurred interest in developing on-chip antennas (OCAs). However, low gain and poor radiation characteristics have been significant challenges. Integrating an artificial magnetic conductor (AMC) into the oxide layer is an alternative. This article presents a new AMC model that improves the performance of 28 GHz OCA using dual-rectangular-patch (DRP) as unit cells. The DRP parameters, patch width (Pw), patch gap (Pg), and substrate height (hs) were used to control the AMC characteristic. Two numerical equations for gain (G) and efficiency (η) have been developed to evaluate the new model's performance. The impact of parameters on the antenna's gain and radiation efficiency was equally analyzed. A prototype antenna was fabricated and tested to validate the model. It demonstrated a peak gain of 3.69 dB and radiation efficiency of 67.18%, with an achieved impedance bandwidth of 1.27 GHz, making it well-suited for 28 GHz device applications. Furthermore, the equations formulated provide the research community with a straightforward method to calculate the gain and efficiency of a 28 GHz antenna. This method is not limited to OCA but can also be applied to off-chip antennas if DRP-AMC is implemented.

Corresponding Author:

Mohd Fadzil Ain
School of Electrical and Electronic Engineering, Universiti Sains Malaysia
Engineering Campus, 14300 Nibong Tebal, Pulau Pinang, Malaysia
Email: eemfadzil@usm.my

1. INTRODUCTION

In recent years, significant progress has been made in developing chip-based wireless systems, spurred by new applications requiring high data rates, cost-effectiveness, compact sizes, and material stability [1]. This growing demand has incited the development of on-chip antennas (OCA) technology across various application domains. OCA technology is favored for its advantages, such as compact size, high speed, and low energy requirements [2], [3]. It represents a modern chip-based antenna design integrating radio frequency (RF) front-end circuits on the same silicon (Si) chip [4]. It supports large wireless devices operating in the lower and high-frequency bands [5], a promising antenna for smart devices and future technologies [6]. OCA requires a footprint chip for integration and is typically configured in a multi-layer structure made of metal-insulator-semiconductor (MIS) [7]. However, it faces significant setbacks, such as low gain, poor efficiency, and distorted radiation characteristics due to the Si's low resistivity and high permittivity properties [8], [9]. These challenges have prompted considerable efforts to overcome them, as gain and radiation efficiency are crucial

factors in OCA design. Researchers have investigated numerous approaches to enhance the performance of an OCA, such as dielectric resonator antenna (DRA), low back etching (LBE), substrate thinning, artificial dielectric loading (ADL) and the insertion of periodic metasurface including partially reflective surface (PRS), artificial magnetic conductor (AMC). However, materials incompatibilities, cost implications, and large chip-size requirements of some of the techniques [5], [7] lead to the consideration of an AMC due to its cost-effectiveness, which requires no additional substrate and ease of integration [4], [5].

AMCs have been broadly studied over the last years due to their ability to mitigate the challenges posed by the low resistivity and high permittivity of Si substrates, thereby enhancing the antenna's gain and radiation characteristics [10]-[12]. They have artificially created a periodic metasurface with a high-impedance surface to exhibit in-phase reflection [13], [14]. AMCs are two-dimensional periodic surfaces created with grounded frequency selective surfaces (FSS) [15]. They play a significant role in shielding the migrating incidence waves from penetrating lossy Si substrates. The created high impedance surface isolates by reflecting the striking signal propagated from the radiating, thereby improving the radiation into the air [11]. Hence, the operation of AMCs can be effectively described using the transmission line (TL) theory. The main requirement for an AMC is to achieve the highest possible reflection coefficient when the surface is illuminated by a migrating incidence wave, which can be expressed as (1) [16]:

$$\Gamma(\omega, \phi, \theta) = \frac{Z_s(\omega, \phi, \theta) - \eta_0}{Z_s(\omega, \phi, \theta) + \eta_0} \tag{1}$$

where Γ is the reflection coefficient, $Z_s(\omega, \phi, \theta)$ denote the total impedance of the structure, which varies with the angle of incidence (θ), frequency (ω), and polarization (ϕ).

Previous research has employed different geometrical configurations of AMC to improve gain, radiation efficiency, and radiation patterns of OCA. For example, a meandered bowtie integrated OCA with a dual dipole patch AMC was introduced in [17], achieving a gain increase from 4.15 to 4.93 dB compared to a single-dipole model. Another study developed a square-loop structured AMC embedded in a six-layer OCA model [11], achieving an intrinsic gain of -1.4 dB, an 8 dB improvement over non-AMC antennas. Additionally, an H-shaped AMC integrated into an OCA is detailed in [10], showing a 19% efficiency improvement and a 0.77 dB increase in peak gain compared to non-AMC designs.

For an AMC to function efficiently, it is essential to control its properties like reflection coefficient, reflection phase, and bandwidth, which have often been not considered in the earlier designs of AMC-inspired OCA. However, similar investigations have been presented for off-chip antennas. Therefore, maintaining a consistent dielectric thickness and periodicity (unit-cell geometry) is crucial for stable AMC performance [18]. Generally, AMCs are limited in their operating frequency due to inherent resonance characteristics. Their reflection coefficient varies from -180° to +180°, and the limited bandwidth lies within -90° to 90°. Several methods have been suggested to stabilize the AMC characteristic, including using loop-based unit cells (LUC), metal vias, and adding a lumped inductor. A square-LUC design aimed at improving the angular stability of an AMC is proposed [19] by integrating lumped inductors into the structure. The design achieved considerable stabilization as compared with previous studies. In addition, skewed cross-shaped FSSS was introduced to angularly control the AMC properties. As a result, an acceptable bandwidth and good stabilized performance are achieved [12].

This study aims to introduce a new AMC structure using a dual rectangular patch (DRP) unit cell configuration. The DRP-AMC unit cell is modeled, optimized and incorporated into the design to control the characteristics and bandwidth of the AMC, thereby improving the overall performance of the antenna. This approach aims to supplement the technique used in previous work, which involved metal vias and lumped inductors that are challenging to integrate into an OCA, as well as fabrication costs due to the multi-layered structure of OCA. This article is structured to cover the antenna design, configuration, and characteristics of the DRP model in section 2, followed by response surface-based modeling (RSM), experimental setup, and optimization in section 3. Section 4 focuses on the antenna's simulation, measurement, and validation. Hence, the findings are summarized in section 5.

2. ANTENNA DESIGN AND METHOD
2.1. Antenna geometry and configuration
In this section, the concept, design, and procedures for the proposed antenna are explained. The antenna was developed using a multi-layered structure consisting of three metal layers, M1, M2, and M3, of silver material and 1 µm thick each, two layers of silicon-oxide (SiO$_2$) of the dielectric constant of 3.75, and a thickness of 25 µm each, and a silicon substrate of dielectric constant 11.9, 500 µm thick and resistivity of 1-15 Ω-cm. The stacking process was based on the complementary metal oxide semiconductor (CMOS) design principle. A slotted microstrip patch with dimensions of 2.4 mm×3.6 mm×0.001 mm is integrated as the top radiating conductor.

A 3D CST electromagnetic (EM) software is used to design and optimize the proposed model. To validate the simulation results, the antenna prototype was fabricated using direct current (DC) magnetron sputtering technology. Figure 1 illustrates the materials and procedure for developing the antenna.
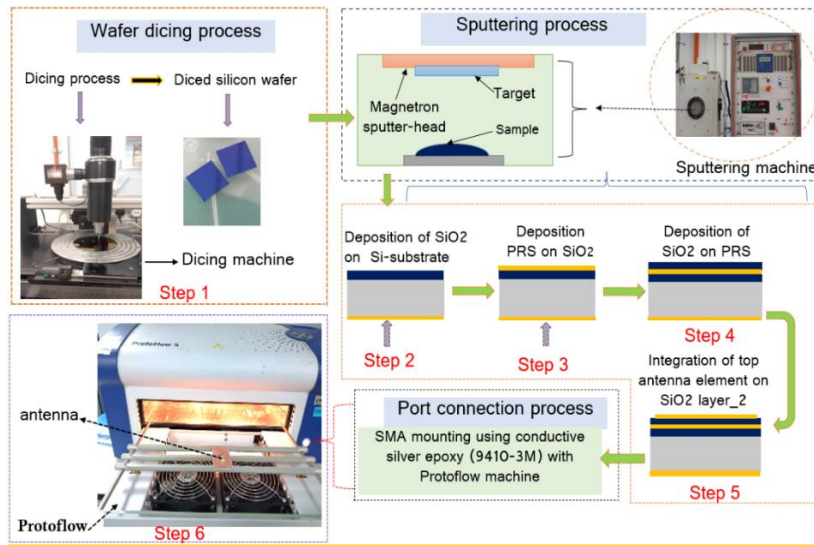

Figure 1. Material and fabrication procedure of the proposed antenna

Figures 2(a) to (d) display the geometrical layout of the complete structure. The slot on the patch in Figure 2(a) is designed to enhance system bandwidth and resonance control, as high-frequency antenna experiences lower bandwidth. The second layer of the stacked structure, depicted in Figure 2(b), is a 500 µm thick silicon substrate. The third and fourth layers are the SiO2, which provide insulation between the top antenna radiating element (M1) (Figure 2(c)) and the 3×3 DRP-AMC structure (M2). The bottom layer (M3) (Figure 2(d)) has dimensions of 10 mm×10 mm and is edged slotted at two center-ends acting as a ground conductor.
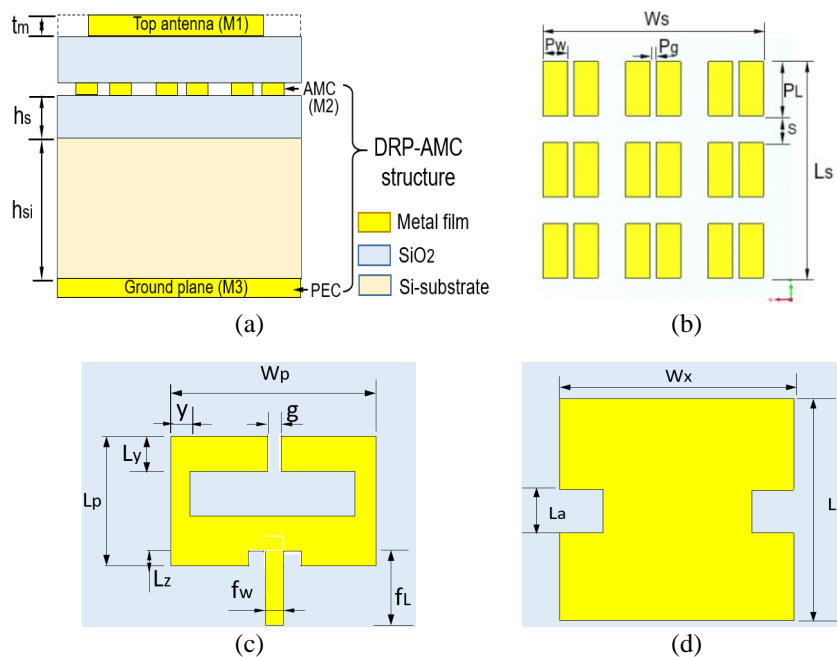

Figure 2. The geometry of the proposed OCA; (a) multi-layer structure, (b) DRP-AMC structure (M2), (c) top antenna element (M1), and (d) perfect ground conductor (M3)

The edge slots are introduced to disperse surface wave generation. The DRP-AMC structure was modelled to perform two functions: to serve as a shield by preventing the EM waves from the top radiating conductor from penetrating the lossy Si substrate due to its low resistivity of (1-15 Ω-cm) and high permittivity properties [20], [21]. Secondly, to control the characteristics of the AMC, thereby increasing the radiation performance and gain of the antenna, compared to conventional AMC design structure with single patch geometry. Consequently, the optimized parameters of the antenna structures in Figure 2 are shown in Table 1, while that of the DRP-AMC is shown in Table 2.

Table 1. Proposed antenna parameters

Parameter	Value (mm)	Parameter	Value (mm)
Substrate width (Ws)	8.50	Metal thickness (tm)	0.001
Substrate length (Ls)	8.92	Feedline width (fw)	0.42
Width of ground plane (Wx)	10	Feedline length (fL)	1.0
Length of ground plane (Lx)	10	Slot gap(g)	0.3
Patch width (Wp)	3.14	Height of Si substrate(hsi)	0.5
Patch length (Lp)	2.36	Length of edge slot (La)	2
Inset length (Lz)	0.27	Height of SiO₂ (hs)	0.025

Table 2. Optimized DRP-AMC parameters

Parameter	Value (mm)
Patch width (Pw)	0.75
Patch length (PL)	2
Patch gap (Pg)	0.5
Substrate length (Ls)	10
Spacing between adjacent unit cell (S)	1
Substrate width (Ws)	10

2.2. Design of dual-rectangular-patch-artificial magnetic conductor model

This section presents the design of DRP-AMC, a new periodic structure of conventional AMC. The parameters of the structure are patch-width (Pw), patch-gap (Pg), and substrate height (hs), as illustrated in Figure 3(a). It is designed to boast not only the gain and radiation efficiency but also control the radiation characteristics of OCA by varying the separation gap Pg. This control capability is absent in the traditional AMC model, where a single patch is typically integrated into a unit cell based on its shape and geometry. The gap introduces capacitance (Cg), while C1 and C2 are parasitic capacitances between the ground conductor and the patches. L1 and L2 represent the inductance of the two patches, and Lg is the inductance of the ground conductor. The equivalent circuit is shown in Figure 3(b). The inductance (L) and capacitance (C) of the AMC can be determined using (1) and (2) [22], whereas the resonance frequency and bandwidth can be calculated using (4) and (5). Figure 3(a) illustrates the DRP-AMC geometry, while Figure 3(b) shows its equivalent circuit model.
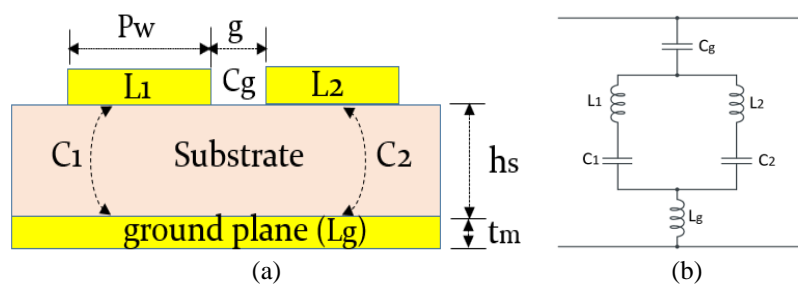

Figure 3. Proposed DRP-AMC model; (a) unit cell and (b) equivalent circuit

$$L = 4\pi x 10^{-7}\mu_r h_s \qquad (2)$$

$$C = 2.82 x 10^{-12}(1 + \varepsilon)\cosh^{-1}\frac{(2P_w - P_g)}{P_g} \qquad (3)$$

$$F = \frac{1}{2\pi\sqrt{LC}} \qquad (4)$$

$$BW = \frac{1}{\eta}\sqrt{\frac{L}{c}} \qquad (5)$$

2.3. Characteristics of the dual-rectangular-patch-artificial magnetic conductor

To achieve the performance of the DRP-AMC presented in Figure 3(a), the model was simulated with a perfect magnetic layer (PML) configuration, as illustrated in Figure 4(a). The findings indicate that the gap between the patch (Pg), the patch width (Pw), and the substrate height (hs) play a essential role in influencing the model's characteristics, especially the reflection phase. Variations in hs change the reflection coefficient and influence the operational frequency, causing it to shift left or right on the frequency axis. Furthermore, the bandwidth (BW) of the model changes when the reflection phase shifts beyond the boundary of -90° to +90°. This change is attributed to increased capacitance C1 and C2, which are inversely proportional to the distance between the AMC and the ground conductor [17].

Consequently, the capacitance Cg changes proportionally with the separation Pg, causing a zero-degree reflection phase at 28 GHz when Pg is between 0.25 mm and 0.3 mm. This phase shift demonstrates the impact of the distance between patch-A and patch-B in the DRP unit cell on reflection phase characteristics, leading to improved antenna gain and radiation resistance. The zero-degree reflection phase characteristic can be achieved at a desired frequency by configuring the unit cell with a PML, as shown in Figure 4(b), with specific boundary conditions on the xy-plane and a Cloquet port along the z-axis at an approximate distance equal to the wavelength (λ).
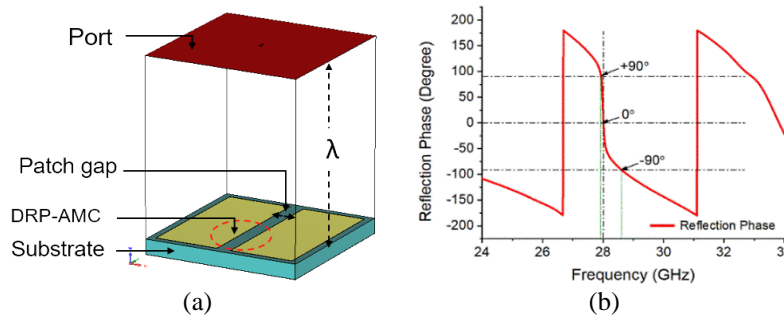

Figure 4. AMC unit cell; (a) PML configuration and (b) reflection phase characteristic

3. RESPONSE SURFACE-BASED MODELING

RSM has been used for various non-linear regression models, such as quadratic, cubic, quartic, and often in higher-order regression models. This work utilized a reduced quartic model (RQM) to establish the output equations, eliminating non-significant high-order variables. This approach is used to approximate both the actual and coded values [23]. In (6) presents the general formula for the non-linear regression function based on the RQM. Where β_o is denoted as the intercept of the polynomial equation, β_1, β_2, and β_3 are coefficients of 4th-order regression, and y is the model output response [24]. Thus, a general formula is represented as (7):

$$y = \beta_o + \sum_{i=1}^{k}\beta_i X_i + \sum_{i=1}^{k}\sum_{j=i+1}^{k}\beta_{ij} X_i X_j + \sum_{i=1}^{k}\beta_{ii} X_i^2 + \ldots\ldots + \beta_{ii} X_i^4 + \varepsilon \qquad (6)$$

$$y = \beta X + \varepsilon \qquad (7)$$

3.1. Variables selection

In OCA-integrated technologies, the device's effectiveness hinges on critical variables that can impact the performance and feasibility of the antenna. This model addresses such needs by incorporating three independent and two response variables. Table 3 levels the experimental factors of the DRP-AMC parameters *Pw*, *Pg*, and *hs*.

Table 3. 3^K level experimental values

Independent factor (mm)	Real value		
	-1	0	1
Patch gap (*Pg*)	0.1	0.250	0.4
Patch width (*Pw)*	0.5	2.250	4
Substrate height (*hs)*	0.025	0.275	0.525

3.2. Design of experiment

As previously stated, an RSM is used to analyze the influence of predictive variables, which are vital for the performance of the AMC structure. These variables are normalized and coded from -1 to +1, with 0 as the midpoint, using (8) to (11). The parameters X_{max} and X_{min} denote the upper and lower limits of the actual size of the DRP-AMC. Y represents the exact size of the independent variable, while X_{cd} stands for the coded value. In this experiment, the actual, maximum, minimum, and coded values for Pg, Pw, and hs can be determined by substituting (9) and (10).

$$X_{cd} = \frac{(Y - x)}{y} \tag{8}$$

$$x = \frac{(X_{max} + X_{min})}{2} \tag{9}$$

$$y = \frac{(X_{max} - X_{min})}{2} \tag{10}$$

$$Y = y.X_{cd} + a \tag{11}$$

Similarly, EM simulation for the factorial level resulted in 20 outcomes and 13° of freedom based on three significant independent variables, keeping patch-length (PL) and dielectric constant, ε_r =11.9 constant. Equally, it is observed that the experimental p-value for the gain and efficiency responses is less than 0.05, indicating that the model is significant and well-suited for determining the optimal AMC-inspired OCA resonating at 28 GHz. Thus, the length of the patch has minimal effect on the characteristic compared to the other key parameters of the model.

3.3. Developed equation

Initially, data obtained from EM simulations were used to construct response models, followed by conducting experimental simulation runs. An ANOVA was then performed to determine the significance of the non-linear regression model adapted for the experiment, identifying a reduced quartic model as the most important. Consequently, the regression model equations for the gain and efficiency of the DRP-AMC were formulated as shown in (12) and (13). The data were experimentally run using these models.

$$\begin{aligned} Gain(dB) = {} & 5.12 - 12.18P_g - 0.76P_w - 0.79h_s + 8.07P_gP_w + 6.83P_gh_s + 0.09P_wh_s + \\ & 25.02P_g{}^2 + 0.13P_w{}^2 - 1.67P_gP_wh_s - 18.28P_g{}^2P_w - 1.33P_gP_w{}^2 + \\ & 3.16P_g{}^2P_w{}^2 \end{aligned} \tag{12}$$

$$\begin{aligned} Efficiency(\%) = {} & 89.03 - 206.26P_g - 12.36P_w - 15.67h_s + 138.68P_gP_w + \\ & 129.25P_gh_s + \; 2.43P_wh_s + 425.66P_g{}^2 + 2.06P_w{}^2 - 31.51P_gP_wh_s - \\ & 319.92P_g{}^2P_w - 25.57P_gP_w{}^2 + 54.98P_g{}^2P_w{}^2 \end{aligned} \tag{13}$$

3.4. Fitness evaluation

The study assessed the model's fitness model by examining the adequacy of the constructed RSM. An ANOVA is used to validate the normality and residual plots of the gain and efficiency, as presented in Table 4, indicating significant responses for both. The model met the criteria for reduced quartic regression and demonstrated significance for both equations, with p-values of 0.0008 for gain and 0.0026 for efficiency, alongside determination coefficients (R^2) of 0.9765 and 0.9647, respectively. Thus, these values confirmed the model's significance, which is crucial for predicting subsequent responses as R2 is close to unity. The parameters A, B, and C and the interactions AB, BC, AC, and cubic and quartic terms exhibited significant effects on both responses, with p-values below 0.05. Parameters C, AB, AC, BC, ABC, A²B, AB², and A²B² emerged as significant models for both gain and efficiency. However, A, B, A², and B², with values above 0.1000, were not considerable model terms in either response.

3.5. Developed model optimization

The article explores the use of non-linear optimization in characterizing OCA, focusing on a set of design parameters derived from non-linear numerical equations. These equations are developed to assess the performance of the DRP-AMC-inspired OCA within the design space. They are optimized to estimate input parameter values not initially obtained in experimental results. This study chooses the desirability function to assess the optimized parameters other than numerical methods as it is used for handling multiple response variables [25]. This approach allows a response model to be converted into a discrete function and identifies the optimal conditions of the variables. The desirability function is expressed as (14):

$$D = ((d_1)^{w_1} + (d_2)^{w_2} \ldots \ldots + (d_n)^{w_n})^{\frac{1}{\Sigma w_i}} \tag{14}$$

where d_1, d_2.... dn, are individual desirability functions of the i- term response with i=1, 2, 3…n, and w_n is the itemized parameters that prioritize the functions. The main goal of this optimization process is to maximize the value of D, a composite function. When all targeted responses ($d_{i,}$=1) reach unity, D achieves its maximum value (D=1). On the other hand, if one or more responses fall outside the predefined limits ($d_{i,}$=0), the desirability function drops to zero. The experiment aims to maximize gain and efficiency responses to achieve a desirability function of unity, with the specific objectives of the DRP-AMC being to optimize gain and radiation efficiency. However, the optimal parameters were Pg=250 µm, Pw=950 µm, and hs=525 µm. These parameters significantly affect the reaction, while the interaction between hs and Pg has a negligible impact on gain and efficiency.

Table 4. Comparison of the proposed design with previous work

Ref	Freq (GHz)	Ant. size (mm)^2	Technology	Peak gain (dB)	Rad. eff (%)	BW (%)
[26]	28	0.25×0.3	65 nm CMOS	-10	45	5.3
[27]	21-40	1.3×0.25	UMC180 nm CMOS	-2	NM	38
[28]	28-33	0.66×0.85	28 nm CMOS	-1.8+2.2	NM	NM
[29]	30	0.75×1.9	130 nm CMOS	-4.3	NM	-
[30]	24	3.8×4	675 µm MIS Si-wafer	-4.5	60-81	5.3
This work	28	2.4×3.4	500 µm, MIS Si-wafer	3.69	67.18	4.32

NM: not mentioned, Si-wafer: silicon wafer, and MIS: metal-insulator-semiconductor

4. RESULTS AND DISCUSSION

In this investigation, simulations of the proposed antenna were carried out using 3D CTS microwave software at an operating frequency of 28 GHz. The parameters, including the magnitude of S11, gain, radiation characteristics, and impedance bandwidth, were studied. The antenna demonstrated a simulated gain of 4.14 dB and a radiation efficiency of 71.2%. To ensure that the simulation results meet the antenna requirements, a prototype of the antenna was fabricated, as presented in Figures 5(a) and (b). The prototype was measured and analyzed using a network analyzer. The results showed a gain of 3.68 dB and radiation efficiency of 67.18%, confirming that the simulation results agree with the experimental measurements. Additionally, the measurement indicated an impedance bandwidth of 1.27 GHz with a return loss below -20 dB.
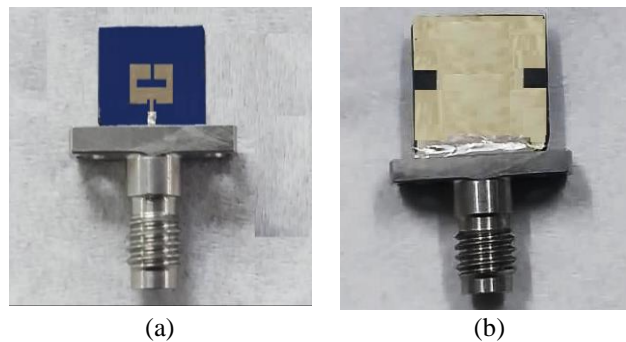

| (a) | (b) |

Figure 5. Fabricated antenna; (a) top view and (b) bottom view

Moreover, Figure 6 compares the simulation and experimentally measured return loss, and a good agreement between the two results is observed. However, minor differences in impedance bandwidth are observed, which could be attributed to factors such as fabrication tolerances, impedance mismatches, and dielectric losses. In addition, the measured gain and the radiation efficiency for the suggested antenna with DRP-AMC and with single patch AMC were equally verified. The results indicate that the proposed antenna realized a peak gain of 3.68 dB, along with a calculated radiation efficiency of 68.17%. Consequently, the suggested antenna achieved an increased gain of 1.32 dB and an efficiency of 15.68% compared to the single patch AMC. The comparison of the antenna with DRP-AMC and with single patch AMC are presented in Figures 7(a) and (b). This enhancement is attributed to the DRP-AMC's ability to boost the gain and radiation performance of the OCA.
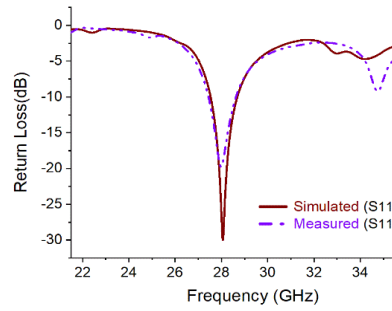
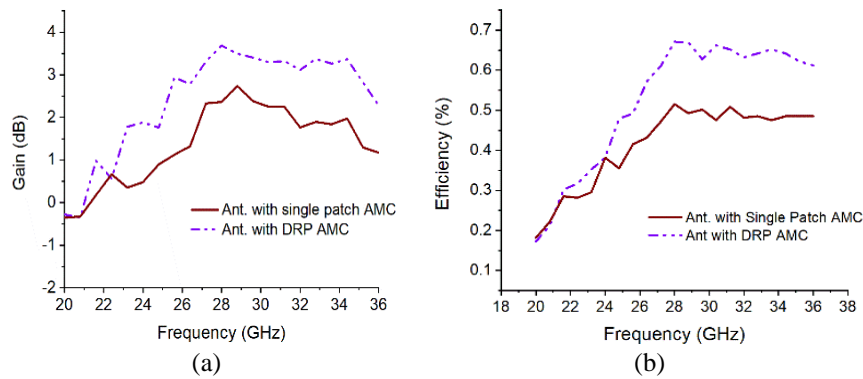Figure 6. The simulated and measured S-parameter of the antenna at 5.8 GHz

Figure 7. The gain and radiation efficiency; (a) gain and (b) efficiency

The far-field radiation characteristics of the suggested antenna have been equally studied. Figures 8(a) and (b) show the simulation and measured radiation pattern representation in E- and H-plane. The result showed good with minor divergences between the simulated and measured co-polarization, but a significant difference between co- and cross-polarization was observed. Hence, this is an indication that losses due to path, capable and inferences were minor. It means the antenna achieved good operation performance.
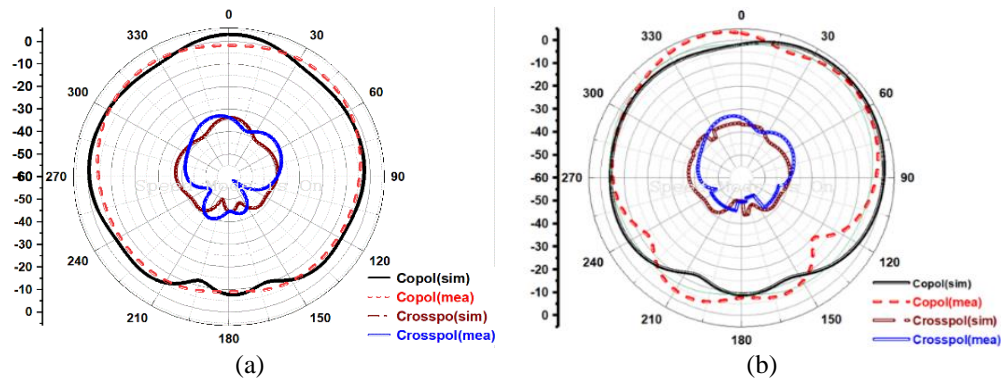
Figure 8. Comparison of simulated and measured far-field radiation; (a) E-plane and (b) H-plane

Additionally, the suggested antenna was designed and optimized utilizing the parameters of DRP-AMC: Pg, Pw, and hs. The entire structure was simulated, and the results were used to develop the response model. Consequently, numerical equations for gain and radiation efficiency were formulated, as presented in (12) and (13). These equations can be used to achieve the peak gain and radiation efficiency by optimizing these parameters. The equations iteratively validated for difference values of Pg, Pw, and hs, resulting in a peak gain of 4.1 dB and radiation efficiency of 70.2% at the optimized value of Pg=250 µm, Pw=950 µm, and hs=525 µm.

These results closely matched the simulated values and agreed with the measured data. The antenna performance can be improved by further optimizing these parameters.

The parametric study on the effect of the model performance was carried out, and Pg had the most significant impact on the characterization of developed equations compared to Pw and hs. Figure 9 presents the parametric characteristics of the reflection phase for Pg values of 0.10 mm, 0.15 mm, 0.20 mm, 0.25 mm, and 0.30 mm. The characteristic plot indicated that raising the value of Pg impacts the reflection phase and elevates the resonance frequency.
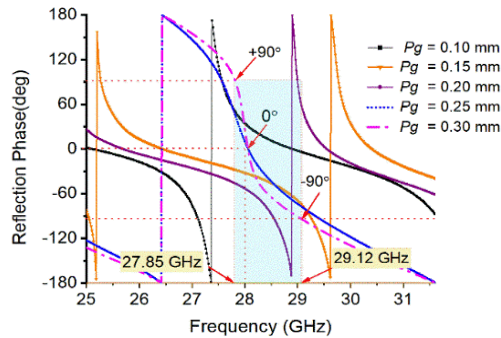
Figure 9. Effect on separation gap, Pg on the reflection phase

Table 4 enlisted the significant parameters of the proposed antenna in comparison with the suggested work in the previous studies. Despite the compactness of the suggested antennas in [26]-[29], it is realized that the reported gain is low compared to the proposed design in this work. However, Elsheakh and Shawkey [27] achieved an outstanding bandwidth of 38%, which is highly impressive. The proposed antenna in [30] achieved the highest efficiency obtained compared to the enlisted works. However, despite the large antenna size of 3.8×4 mm^2, it achieved a low gain in comparison with the proposed work. When compared to the suggested works, it is clear that the proposed antenna achieved significant performance, especially the gain and radiation efficiency, as well as the developed model equations, which is an added advantage.

5. CONCLUSION

This article introduces a DRP-AMC-inspired OCA for 28 GHz device applications for the first time. Extensive analysis of simulation results shows that incorporating the new AMC structure has significantly impacted the OCA's performance. It achieves a maximum gain of 3.69 dB and radiation efficiency of 67.18%, which showcases an improvement of 35.7% in gain and 23.3% in efficiency over conventional single square patch AMC-inspired OCA. Moreover, the antenna demonstrates a considerable bandwidth of 1.27 GHz, from 27.85 GHz to 29.12 GHz. Two model equations for gain and radiation efficiency were developed and analyzed to validate the simulation results. Optimal gain and radiation efficiency were achieved with DRP-AMC parameters of Pg=250 µm, Pw=950 µm, and hs=525 µm. An antenna prototype was subsequently fabricated and tested to validate the accuracy of the simulation and model results. With a radiator footprint size of $2.36\times3.14\times0.55$ mm³, the achieved gain and bandwidth make this antenna suitable for integration into 28 GHz wireless transceivers. The developed model equation can also be adjusted for future designs to operate at frequencies other than 28 GHz.

REFERENCE

[1] B. Sene, D. Reiter, H. Knapp, and N. Pohl, "Design of a cost-efficient monostatic radar sensor with antenna on chip and lens in package," *IEEE Trans. Microw. Theory Tech*, vol. 70, no. 1, pp. 502–512, 2022, doi: 10.1109/TMTT.2021.3098862.
[2] Z. Chen, Q. Liu, B. Smolders, P. Baltus, and H. Gao, "30-GHz co-designed low-noise amplifier and antenna-on-chip for wireless applications," *2019 IEEE International Symposium on Radio-Frequency Integration Technology (RFIT),* 2019, pp. 5–7, doi: 10.1109/RFIT.2019.8929159.

[3]   S. Juneja, R. Pratap, and R. Sharma, "Semiconductor technologies for 5G implementation at millimeter wave frequencies – design challenges and current state of work," *Engineering Science and Technology, an International Journal,* vol. 24*,* no. 1, pp. 205-217, 2021, doi: 10.1016/j.jestch.2020.06.012.

[4]   R. Karim, A. Iftikhar, B. Ijaz, and I. B. Mabrouk, "The potentials, challenges, and future directions of on-chip-antennas for emerging wireless applications—a comprehensive survey," *IEEE Access*, vol. 7, pp. 173897–173934, 2019, doi: 10.1109/ACCESS.2019.2957073.

[5]   H. M. Cheema and A. Shamim, "The last barrier: on-chip antennas," *IEEE Microwave Magazine*, vol. 14, no. 1, pp. 79–91, Jan. 2013, doi: 10.1109/MMM.2012.2226542.

[6]   H. Zhu, X. Li, Z. Qi, and J. Xiao, "A 320 GHz Octagonal shorted annular ring on-chip antenna array," *IEEE Access*, vol. 8, pp. 84282–84289, 2020, doi: 10.1109/ACCESS.2020.2991868

[7]   A. Shamim, H. M. Cheema, and F. Khalid, *Antenna-on-chip; design, challenges, and opportunities*, Artech House, Norwood, 2021.

[8]   R. K. Kushwaha, P. Karuppanan, and R. K. Dewang, "Design of a SIW on-chip antenna using 0.18-μm CMOS process technology at 0.4 THz," *Optik (Stuttg).,* vol. 223, no. June, p. 165509, 2020, doi: 10.1016/j.ijleo.2020.165509.

[9]   H. Singh, S. Mandal, S. K. Mandal, and A. Karmakar, "Design of miniaturized meandered loop on-chip antenna with enhanced gain using shorted partially shield layer for communication at 9.45 GHz," *IET Microwaves, Antennas & Propagation.*, vol. 13, no. 7, pp. 1009–1016, 2019, doi: 10.1049/iet-map.2018.5974.

[10]   H. T. Huang, B. Yuan, X. H. Zhang, Z. F. Hu, and G. Q. Luo, "A circular ring-shape monopole on-chip antenna with artificial magnetic conductor*, in 2015 Asia-Pacific Microwave Conference (APMC),* 2015, pp. 3–5, doi: 10.1109/APMC.2015.7413137.

[11]   M. Nafe, A. Syed, and A. Shamim, "Gain-Enhanced on-chip folded dipole antenna utilizing artificial magnetic conductor at 94 GHz", *IEEE Antennas and Wireless Propagation Letters.*, vol. 16, no. c, pp. 2844–2847, 2017, doi: 10.1109/LAWP.2017.2749308.

[12]   M. Hosseini, A. Pirhadi, and M. Hakkak, "Compact angularly stable AMCs utilizing skewed cross-shaped FSSS," *Microwave and Optical Technology Letters*, vol. 49, no. 4, pp. 781–786, 2007, doi: 10.1002/mop.22280.

[13]   Y. Yu, Z. Akhter, and A. Shamim, "Improving the performance of antenna-on-chip by effectively illuminating the artificial magnetic conductors through coupling enhancement structures," *IEEE Transactions on Antennas and Propagation,* vol. 71, no. 5, pp. 4492–4497, 2023, doi: 10.1109/TAP.2023.3239102.

[14]   A. Shamim and H. Zhang, "On-chip antenna: challenges and design considerations, in *Antennas and Propagation for 5G and Beyond,*" Eds. Institution of Engineering and Technology, 2020, pp. 123–155, doi: 10.1049/PBTE093E_ch6.

[15]   V. G. M. Annamdas and C. K. Soh, "Contactless load monitoring in near-field with surface localized spoof plasmons—a new breed of metamaterials for health of engineering structures," *Sensors and Actuators A: Physical,* vol. 244, pp. 156–165, 2016, doi: 10.1016/j.sna.2016.04.037.

[16]   D. M. Pozar, *Microwave Engineering*, 4th ed. John Wiley & Sons, 2009

[17]   N. Othman, N. A. Samsuri, M. K. A. Rahim, and K. Kamardin, "Low specific absorption rate and gain-enhanced meandered bowtie antenna utilizing flexible dipole-like artificial magnetic conductor for medical application at 2.4 GHz," *Microwave and Optical Technology Letters,* vol. 62, no. 12, pp. 3881–3889, 2020, doi: 10.1002/mop.32507.

[18]   M. E. de Cos and F. Las-Heras, "On the advantages of loop-based unit-cell's metallization regarding the angular stability of artificial magnetic conductors," *Applied Physics A*, vol. 118, pp. 699–708, 2015, doi: 10.1007/s00339-014-8782-8.

[19]   H. F. Álvarez, M. E. de Cos, S. García, and F. Las-Heras, "Enhancing the angular stability of artificial magnetic conductors through lumped inductors," *Sensors and Actuators A: Physical*, vol. 272, pp. 223–230, 2018, doi: 10.1016/j.sna.2018.01.026.

[20]   X. S. Yang, S. Koziel, and L. Leifsson, "Computational optimization, modelling and simulation: recent trends and challenges," *Procedia Computer Science*, vol. 18, pp. 855–860, 2013, doi: 10.1016/j.procs.2013.05.250.

[21]   R. Karim, A. Iftikhar, and R. Ramzan, "Performance-issues-mitigation-techniques for on-chip-antennas – Recent developments in RF, MM-Wave, and THz bands with future directions," *IEEE Access*, vol. 8, pp. 219577–219610, 2020, doi: 10.1109/ACCESS.2020.3042928.

[22]   D. H. Margaret and B. Manimegalai, "Modeling and optimization of EBG structure using response surface methodology for antenna applications," *AEU - International Journal of Electronics and Communications,* vol. 89, pp. 34–41, 2018, doi: 10.1016/j.aeue.2018.03.017.

[23]   M. Isafiq, Z. Shayfull, S. M. Nasir, M. M. Rashidi, M. Fathullah, and N. Z. Noriman, "Shrinkage analysis on thick plate part using response surface methodology (RSM)," *2nd International Conference on Green Design and Manufacture 2016 (IConGDM 2016)*, 2016, vol. 78, pp. 0–7, doi: 10.1051/matecconf/20167801084.

[24]   Z. Chen, Y. Xu, C. Wang, Z. Wen, Y. Wu, and R. Xu, "A Large-signal statistical model and yield estimation of GaN HEMTs based on response surface methodology," *IEEE Microwave and Wireless Components Letters,* vol. 26, no. 9, pp. 690–692, 2016, doi: 10.1109/LMWC.2016.2597196.

[25]   N. R. Costa, J. Lourenço, and Z. L. Pereira, "Desirability function approach: a review and performance evaluation in adverse conditions," *Chemometrics and Intelligent Laboratory Systems,* vol. 107, no. 2, pp. 234–244, Jul. 2011, doi: 10.1016/j.chemolab.2011.04.004.

[26]   P. Burasa, T. Djerafi, and K. Wu, "A 28 GHz and 60 GHz dual-band on-chip antenna for 5G-compatible IoT-served sensors in standard CMOS process," *IEEE Transactions on Antennas and Propagation*, vol. 69, no. 5, pp. 2940–2945, 2021, doi: 10.1109/TAP.2020.3025236.

[27]   D. Elsheakh and H. Shawkey, "5G wideband on-chip dipole antenna for WSN soil moisture monitoring," *International Journal of RF and Microwave Computer-Aided Engineering,* vol. 31, no. 4, pp. 1–12, Apr. 2021, doi: 10.1002/mmce.22556.

[28]   M. K. Hedayatim *et al.*, "Challenges in on-chip antenna design and integration with RF receiver front-end circuitry in nanoscale CMOS for 5G communication systems," *IEEE Access*, vol. 7, no. December, pp. 43190–43204, 2019, doi: 10.1109/ACCESS.2019.2905861.

[29]   P. Chen and A. Babakhani, "3-D radar imaging based on a synthetic array of 30-GHz impulse radiators with on-chip antennas in 130-nm SiGe BiCMOS," *IEEE Transactions on Microwave Theory and Techniques,* vol. 65, no. 11, pp. 4373–4384, 2017, doi: 10.1109/TMTT.2017.2694826.

[30]   S. Mandal, H. Singh, S. K. Mandal, A. K. Mal, R. Mahapatra, and P. R. T. Naidu, "A 24 GHz circularly polarized on-chip antenna for short-range communication application," *Scientia Iranica*, vol. 30, no. 4, pp. 1314–1329, Aug. 2023, doi: 10.24200/sci.2022.57325.5202.

BIOGRAPHIES OF AUTHORS

Ahmadu Girgiri received a B.Eng. degree in Electrical Engineering from Bayero University Kano, Nigeria in 2008 and an M.Sc. in Information and Communication Technology from the University of Wolverhampton, United Kingdom, in 2013. He is working toward a Ph.D. in Antenna and Propagation at the School of Electrical and Electronic Engineering, Universiti Sains Malaysia, Malaysia. He works with the Department of Electrical and Electronic Engineering, Mai Idris Alooma Polytechnic, Geidam, Yobe-Nigeria. He is a communication and wireless services consultant at Array Digital and Communications, Kano, Nigeria. His research interests include RF and mobile communication, wireless sensor systems, and on-chip design for sub-6 GHz and 5G. He can be contacted at email: ahmadu.g@student.usm.my.

Mohd Fadzil Ain received B.S. degree in Electronic Engineering from University Technologi Malaysia, Malaysia (UTM), 1997; M.S. in Radio Frequency and Microwave from Universiti Sains Malaysia (USM), Malaysia, in 1999; Ph.D. degree in Radio Frequency and Microwave from the University of Birmingham, United Kingdom in 2003; in 2003 he joined the School of Electrical and Electronics Engineering, he is currently a Professor in VK7 Grade, a former Dean of the School of Electrical and Electronic, and the Director of Collaborative Microelectronic Design Excellence Centre (CEDEC), USM. He is Actively Involved in Technical Consultancy with Several Companies in Microwaves Equipment. His research interests include MIMO wireless system FPGA/DSP, Ka-band transceiver design, dielectric antenna, and RF characteristics of dielectric material. His awards and honors include the International Invention Innovation Design and Technology Exhibition, International Exposition of Research and Inventions of Institutions of Higher Learning, Malaysia Technology Expo, Malaysia and many more. He can be contacted at email: eemfadzil@usm.my.

Mohd Zamir Pakhuruddin received a B.Eng. in Electrical Engineering from the University of Sheffield, United Kingdom. He spent about 8 years as a Senior Photolithography and Sputtering (R&D) Engineer in SilTerra and Fuji Electric, Kulim Hi-Tech Park, respectively. In 2012, he graduated with an M.Sc. in Physics at Universiti Sains Malaysia (USM), where he researched silicon thin-film solar cells on flexible substrates. In 2016, he obtained his Ph.D. in Photovoltaic Engineering from the University of New South Wales (UNSW), Australia, where he worked on the development of light-trapping schemes in e-beam evaporated laser-crystallized silicon thin-film solar cells on glass superstrates. He is currently an Associate Professor. He is a Director at the Institute of Nano Optoelectronics Research and Technology (INOR) and a lecturer at the School of Physics, Universiti Sains Malaysia. His research includes black silicon, perovskite, organic, and thin-film solar cells for conventional solar windows, optoelectronic devices, and indoor photovoltaic applications. He can be contacted at email: zamir@usm.my.

Mohamad Faiz Mohamed Omar received his B.Eng. degree (Hons.) in Electronic Engineering and an M.Sc. degree in RF Microwave Engineering from USM, Nibong Tebal, in June 2014 and 2017, respectively. He is currently a research officer at the Collaborative Microelectronic Design Excellence Centre (CEDEC), USM, perusing a Ph.D. in Electrical Engineering, at Universiti Technologi Malaysia (UTM). His current research interests include the simulation and design of high RF and high-power devices, microwave tomography, and digital image processing. He can be contacted at email: faiz_omar@usm.my.

Bello Muhammad Abdullahi received his B.Eng. degree in Electrical and Electronic Engineering from Kwara State University Nigeria, an M.Sc. degree in Electrical and Electronic Engineering from Coventry University United Kingdom (UK), in 2015, and is currently pursuing a Ph.D. degree in Electrical and Electronic Engineering at the University of Sains, Malaysia. His research interests include printable antennas, multiband antenna, and millimeter-wave antennas. He can be contacted at email: engr.mbabdullahi@student.usm.my.